^{18}O-induced single-nucleon transfer reactions on ^{40}Ca at 15.3A MeV within a multichannel analysis

S. Calabrese,[1,2,*] M. Cavallaro,[1] D. Carbone,[1] F. Cappuzzello,[1,2] C. Agodi,[1] S. Burrello,[3,4] G. De Gregorio,[5,6] J. L. Ferreira,[7] A. Gargano,[5] O. Sgouros,[1] L. Acosta,[8,9] P. Amador-Valenzuela,[10] J. I. Bellone,[1] T. Borello-Lewin,[11] G. A. Brischetto,[1,2] D. Calvo,[12] V. Capirossi,[12,13] E. R. Chàvez Lomelì,[8] I. Ciraldo,[1,2] M. Colonna,[1] F. Delaunay,[1,2,14] H. Djapo,[15] C. Eke,[16] P. Finocchiaro,[1] S. Firat,[17] M. Fisichella,[1] A. Foti,[9] M. A. Guazzelli,[18] A. Hacisalihoglu,[19] F. Iazzi,[12,13] L. La Fauci,[1,2] J. A. Lay,[4,20] R. Linares,[7] J. Lubian,[7] N. H. Medina,[11] M. Moralles,[21] J. R. B. Oliveira,[11] A. Pakou,[22] L. Pandola,[1] H. Petrascu,[23] F. Pinna,[12,13] G. Russo,[9] S. O. Solakci,[17] V. Soukeras,[1,2] G. Souliotis,[24] A. Spatafora,[1,2] D. Torresi,[1] S. Tudisco,[1] A. Yildirim,[17] and V. A. B. Zagatto[7]

(NUMEN Collaboration)

[1]*Istituto Nazionale di Fisica Nucleare, Laboratori Nazionali del Sud, Catania, Italy*
[2]*Dipartimento di Fisica e Astronomia "Ettore Majorana", Università di Catania, Catania, Italy*
[3]*Institut für Kernphysik, Technische Universität Darmstadt, Darmstadt, Germany*
[4]*Departamento de Física Atomica, Molecular y Nuclear, Universidad de Sevilla, Sevilla, Spain*
[5]*Istituto Nazionale di Fisica Nucleare, Sezione di Napoli, Napoli, Italy*
[6]*Dipartimento di Matematica e Fisica, Università della Campania "Luigi Vanvitelli", Caserta, Italy*
[7]*Instituto de Física, Universidade Federal Fluminense, Niterói, Brazil*
[8]*Instituto de Física, Universidad Nacional Autónoma de México, Mexico City, Mexico*
[9]*Istituto Nazionale di Fisica Nucleare, Sezione di Catania, Catania, Italy*
[10]*Departamento de Aceleradores y Estudio de Materiales, Instituto Nacional de Investigaciones Nucleares, Ocoyoacac, Mexico*
[11]*Instituto de Física, Universidade de São Paulo, São Paulo, Brazil*
[12]*Istituto Nazionale di Fisica Nucleare, Sezione di Torino, Torino, Italy*
[13]*DISAT, Politecnico di Torino, Torino, Italy*
[14]*LPC Caen, Normandie Université, ENSICAEN, UNICAEN, CNRS/IN2P3, Caen, France*
[15]*Institute of Accelerator Technologies, Ankara University, Ankara, Turkey*
[16]*Department of Mathematics and Science Education, Akdeniz University, Antalya, Turkey*
[17]*Department of Physics, Akdeniz University, Antalya, Turkey*
[18]*Centro Universitario FEI, São Bernardo do Campo, Brazil*
[19]*Institute of Natural Sciences, Karadeniz Teknik Universitesi, Trabzon, Turkey*
[20]*Instituto Interuniversitario Carlos I de Física Teórica y Computacional (iC1), Sevilla, Spain*
[21]*Instituto de Pesquisas Energeticas e Nucleares IPEN/CNEN, São Paulo, Brazil*
[22]*Department of Physics, University of Ioannina and Hellenic Institute of Nuclear Physics, Ioannina, Greece*
[23]*Institutul National pentru Fizica si Inginerie Nucleara Horia Hulubei, Bucarest, Romania*
[24]*Department of Chemistry, University of Athens and Hellenic Institute of Nuclear Physics, Athens, Greece*

(Received 14 September 2021; accepted 16 November 2021; published 10 December 2021)

Background: Nucleon transfer reactions are selective tools for nuclear physics investigations. The theoretical and computational limits affecting in the past their data analysis could be nowadays surmounted thanks to the advent of methods with refined approximations and constraints, even when heavy-ion collisions are considered.
Purpose: Modern microscopic calculations of heavy-ion-induced transfer reactions combined with precise experimental data offer the chance for accurately testing different reaction models as well as the nuclear structure description of the involved nuclear states.
Method: Single proton and neutron transfer reactions were measured with the MAGNEX magnetic spectrometer for the $^{18}\mathrm{O}+{}^{40}\mathrm{Ca}$ system at 15.3A MeV. Excitation energy spectra and angular differential cross section distributions were extracted. The experimental results are compared with theoretical calculations performed in distorted wave and coupled channel Born approximation. The use of a coupled channel equivalent polarization potential to effectively describe the coupling effects affecting the initial state interaction is also considered. Spectroscopic amplitudes derived from a large-scale shell model with appropriate interactions adapted for the involved nuclei are employed.
Results: Our theoretical calculations are in good agreement with experimental data, without the need for any scaling factor, validating the adopted reaction and nuclear structure parameters. Moreover, under the present

*calabrese@lns.infn.it

experimental conditions, a weak dependence of the obtained results on the choice of the reaction models was observed.

Conclusions: The good agreement between experimental and theoretical results validates the reliability of the parameter sets entering the calculations. They are extracted from or tested in complementary analyses of other reaction channels under the same experimental conditions. Such a multichannel approach represents the best option to pursue a solid, comprehensive, and model-independent description of the single-nucleon transfer reactions. The successful description of the present one-nucleon transfer data is also propaedeutic to the accurate assessment, under the same theoretical description, of higher-order transfer processes, like the sequential nucleon transfer mechanisms which are in competition with the direct charge exchange reactions.

DOI: 10.1103/PhysRevC.104.064609

I. INTRODUCTION

Nucleon transfer reactions have historically played a significative role among direct nuclear reactions. One-nucleon transfer processes are, in fact, suitable tools to investigate the single-particle property of the populated nuclear states [1–3] while two-nucleon transfer ones selectively probe pairing correlations in atomic nuclei [4–6]. In the past, however, limitations from the adopted theoretical approximations and the parameters entering in the reaction calculations have often affected the final conclusions of the performed studies. This has frequently prevented to get agreement between measured and calculated cross sections [7–11]. Nowadays, improvements in the theoretical models and computational capabilities allow to tackle nucleon transfer reactions with an unprecedented level of accuracy [12,13], even when medium-mass and heavy ions are considered [14,15]. In this view, transfer reactions represent the ideal ground to test the different nuclear structure models.

High precision results are imperative when considering nucleon transfer reactions as part of more complex reaction networks. One- and two-nucleon transfer reactions, indeed, are among the main competitive processes of direct heavy-ion charge exchange reactions, both single (SCE) and double (DCE). Multinucleon transfer processes, in fact, can also feed the same final nuclear states populated by SCE and DCE reactions. Such transfer contributions to charge exchange reaction channels have already been investigated in the past [16–23]. The main conclusion was that the competition between the direct and nucleon transfer driven charge exchange reactions can vary, changing kinematic conditions and involved nuclei. Thus, the topic can be considered still open for those nuclear systems that have not been investigated yet.

Furthermore, the charge exchange reactions are the object of a renewed extensive interest. In particular, the NUMEN project [24–27] aims at investigating the possible connection between the nuclear matrix elements of the heavy-ion-induced DCE reactions and the double β decay. To this extent, only the direct charge exchange reaction cross sections mediated by the in-medium nucleon-nucleon interaction are of primary interest [28,29]. Thus, such contributions have to be disentangled from the ones due to the multinucleon transfer mechanisms induced by the nuclear mean-field interaction [30]. Although multinucleon transfer driven DCE cannot be totally avoided, it is important to find the conditions that favor the dominance of the direct mechanisms. In this view, also one- and two-nucleon transfer reactions are measured within the NUMEN experimental runs, in the same experimental conditions of the investigated DCE reactions. A successful description of the available nucleon transfer reaction channels represents, in fact, the utmost elements to constrain the analysis of the complete multinucleon transfer processes which are in competition with the direct charge exchange mechanisms.

The theoretical analysis for the transfer reactions can be performed within the distorted wave Born approximation (DWBA) framework. In this scheme, however, the couplings with the excited states in the initial partition are neglected. Such couplings could significantly affect, in principle, the transfer mechanisms, especially when heavy-ion collisions are considered. To properly take into account such effects, coupled channel methods can be invoked, such as resorting to the well-known coupled channel Born approximation (CCBA) scheme [31]. In this view, an alternative is represented also by the coupled channel equivalent polarization (CCEP) potential approach [32,33]. The latter is an effective technique able to incorporate the inelastic coupling effects in the DWBA framework by properly modifying the adopted optical potential. Thus, it may be interesting in more involved reaction studies, where such couplings and their effects cannot be explicitly incorporated.

The nucleon transfer predictions provided within all the mentioned theoretical frameworks are sensitive to few but crucial ingredients, which have to be properly chosen. In particular, the most important quantities are the optical potentials introduced to model the initial and final state interactions among the colliding nuclei and the spectroscopic amplitudes which account for the structure properties of the involved systems. The nuclei typically adopted as projectiles in nucleon transfer reaction studies vary from light to heavy systems. In the present article the one-neutron stripping and one-proton pickup transfer reactions for the $^{18}\mathrm{O}+{}^{40}\mathrm{Ca}$ system at 15.3A MeV are investigated. The $^{18}\mathrm{O}$ has already been considered as a probe for intermediate-mass nuclei [34–37], demonstrating a selective population of single-particle components in bound and resonant states. In Ref. [38], in particular, some nucleon transfer channels were already analyzed for the $^{18}\mathrm{O}+{}^{40}\mathrm{Ca}$ system, even if at lower bombarding energy. The experimental results there obtained, however, were not in excellent agreement with the theoretical calculations, thus motivating a modern investigation for such a system. In our perspective, moreover, the analysis of the ($^{18}\mathrm{O}$, $^{19}\mathrm{F}$) one-proton and ($^{18}\mathrm{O}$, $^{17}\mathrm{O}$) one-neutron transfers completes the examination of all the interesting reaction channels experimentally

investigated in the NUMEN runs for the ^{40}Ca target at the incident energy of 15.3A MeV. This already includes the elastic and inelastic scattering, the two-neutron and two-proton transfers, as well as the SCE and DCE reactions [28,39–42].

The paper is organized as follows. In Sec. II the experimental setup and the data reduction procedure are presented. In Sec. III the theoretical models and the corresponding parameters adopted to perform the one-nucleon transfer cross section calculations are described. In Secs. IV and V the one-neutron stripping and the one-proton pickup results are discussed, respectively. In Sec. VI the conclusions of the present work are drawn and the future perspectives commented.

II. EXPERIMENTAL SETUP AND DATA REDUCTION

The experiment was performed at the INFN-LNS laboratory in Catania. The ^{18}O beam was accelerated by the K800 Superconducting Cyclotron at the energy of 15.3A MeV and transported to the MAGNEX experimental hall preserving its good optical characteristics [43]. The 250 ± 12 μg/cm^2 ^{40}Ca target, manufactured by evaporation onto a carbon backing of 47 μg/cm^2 by the INFN-LNS Target Laboratory, was kept in vacuum until its placement in the MAGNEX scattering chamber to minimize the oxidation phenomena. The $^{18}O^{8+}$ beam was intercepted by a Faraday cup located 15 cm downstream of the target and equipped with a -200 V suppressor ring to measure, with an accuracy better than 10%, the incident ion flux. The MAGNEX spectrometer optical axis was set at 8° in the laboratory frame thus spanning the $3° < \theta_{lab} < 14°$ angular range. The ^{19}F and ^{17}O ejectiles were momentum analyzed by MAGNEX and then measured by its focal plane detector [44,45]. Thanks to the large acceptance in momentum of the spectrometer [43], the two investigated reaction channels, the (^{18}O, ^{17}O) one-neutron stripping and the (^{18}O, ^{19}F) one-proton pickup, were measured under the same experimental conditions, namely, in the same experimental runs within a unique magnetic setting. The data reduction in terms of particle identification and ejectile trajectory reconstruction was performed following the techniques described in Refs. [46–50], finally deducing the scattering angle and the excitation energy distributions.

The excitation energy spectra of the two reaction channels under study are shown in Figs. 1 and 2, where $E_x = Q_0 - Q$ is the difference between the Q values corresponding to the ground and the given excited states. Examining the spectra, both of them present clear peaks and structures; thus they were further analyzed in order to distinguish among the different possible transitions. In more detail, a fit procedure was performed considering the spectra in angular steps of 0.5° or 1°, depending on the available collected statistics.

An example of the one-neutron transfer excitation energy spectrum is shown in Fig. 1. The distribution up to 4 MeV is described by five Gaussian functions corresponding to as many visible structures. The first and the second ones correspond to the transitions to the ground state (g.s.) and the first excited state of the ^{17}O ejectile at 0.871 MeV, respectively. In fact, the energy resolution of about 600 keV full width at half maximum allows to distinguish the two contributions, although they are not fully separated also because the excited

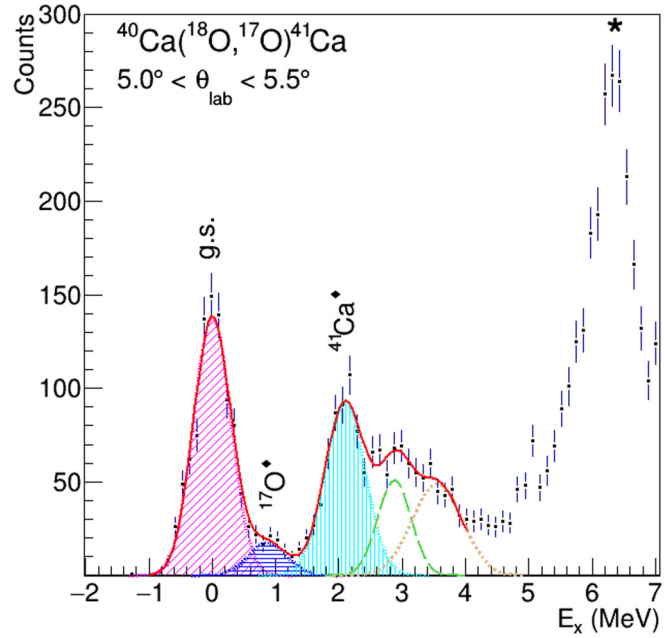

FIG. 1. Excitation energy spectrum for the (^{18}O, ^{17}O) one-neutron stripping reaction in the $5.0° < \theta_{lab} < 5.5°$ angular range. The visible structures up to ≈4 MeV are fitted by a global curve (solid red line) given by the sum of five Gaussian functions; the first two (the diagonally shaded magenta and the horizontally shaded blue) correspond to single transitions while the third one (the vertically shaded cyan) corresponds to the excitation of two different ^{41}Ca excited states (see Table I). The auxiliary Gaussian functions that peak beyond 2 MeV (dashed green and dotted orange) are introduced to better reproduce the shape in such a region. The peak labeled with an asterisk is polluted by target contamination contributions.

state yield is considerably smaller than the g.s. one. The third visible bump around 2 MeV is expected to be the sum of the two transitions to the ^{41}Ca states at 1.942 and 2.010 MeV (see Table I). To better reproduce the spectrum shape in such an energy region, fourth and fifth auxiliary Gaussian functions were introduced to model the visible bumps observed around 3 and 3.5 MeV which, however, are not considered in the present analysis. The higher excitation energy structure shown in the spectrum is dominated by the oxygen and carbon target contaminations, so it will not be analyzed in the following.

Figure 2 shows the excitation energy spectrum up to 5 MeV in a selected angular range for the one-proton transfer reaction channel. It was fitted including four Gaussian functions corresponding to as many low-lying peaks. In particular, peak 1 and peak 2 are expected to receive contributions from the population of few states of the ^{19}F ejectile only, while peak 3 and peak 4 involve several possible transitions of both the ejectile and the ^{39}K residual nuclei (see Table II). However, such clear structures and the corresponding widths, approximately comparable with the ones expected in case of individual transitions, point to a condition of a single or a very few states' dominance. Higher excitation energy bumps visible in the reported spectrum are polluted by oxygen and carbon target contaminations, so they will not be included in the present analysis.

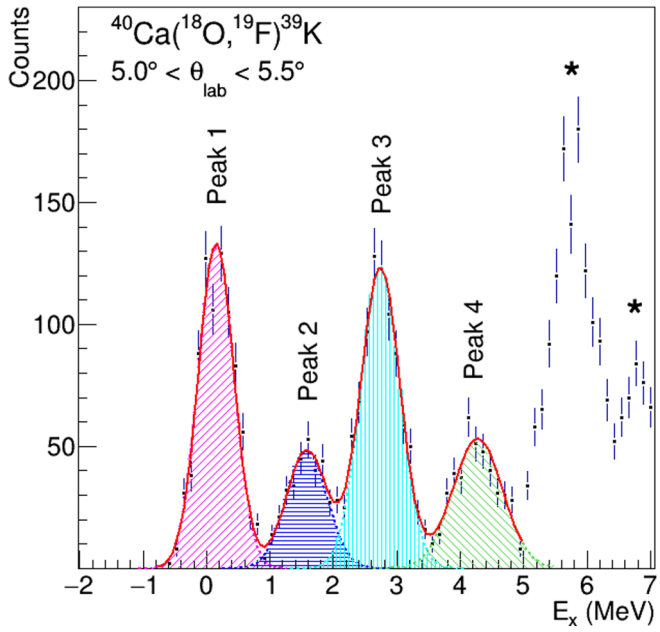

FIG. 2. Excitation energy spectrum for the (^{18}O, ^{19}F) one-proton pickup reaction in the $5.0^\circ < \theta_{\rm lab} < 5.5^\circ$ angular range. The visible structures up to ≈5 MeV are fitted by a global curve (solid red line) given by the sum of four Gaussian functions, each of them accounting for several different transitions (see Table II for the details). The peaks labeled with asterisks are polluted by the target contamination contributions.

Figures 3 and 4 show the extracted angular differential cross section distributions for the one-neutron and one-proton transfer, respectively. The error bars reported in the plots include the statistical contribution and for the cross section angular distributions the uncertainties due to the solid angle evaluation and the fit procedure. The cross section values could be affected by a systematic error estimated as about 10%, generated by the target thickness and the charge collection uncertainties, not reported in the plots.

III. ONE-NUCLEON TRANSFER REACTION CALCULATIONS

One-nucleon transfer reactions can be described in a fully quantum microscopic approach under some assumptions [51]. In the case of single-nucleon transfer between the initial ($\alpha = a + A$) and the final ($\beta = b + B$) partitions, the transition amplitude can be expressed in DWBA as

$$T = \int d\vec{r}_\alpha d\vec{r}_\beta \chi_\beta^{(-)} \langle \psi_B | \psi_A \rangle V_{\alpha,\beta} \langle \psi_b | \psi_a \rangle \chi_\alpha^{(+)}, \qquad (1)$$

where $\chi_{\alpha,\beta}^{(\pm)}$ are the outgoing and incoming distorted waves in the entrance and exit partitions, $V_{\alpha,\beta}$ is a suitable effective

TABLE I. List of the considered final partition channels populated in the experimentally observed structures of the ^{40}Ca(^{18}O, ^{17}O) ^{41}Ca one-neutron transfer excitation energy spectrum of Fig. 1.

Label	Final partition
g.s.	^{17}O g.s. $(5/2^+) + {}^{41}$Ca g.s. $(7/2^-)$
^{17}O ♦	^{17}O$_{0.871}$ $(1/2^+) + {}^{41}$Ca g.s. $(7/2^-)$
^{41}Ca ♦	^{17}O g.s. $(5/2^+) + {}^{41}$Ca$_{1.942}$ $(3/2^-)$
	^{17}O g.s. $(5/2^+) + {}^{41}$Ca$_{2.010}$ $(3/2^+)$

TABLE II. List of the considered final partition channels populated in the experimentally observed structures of the ^{40}Ca(^{18}O, ^{19}F) ^{39}K one-proton transfer excitation energy spectrum of Fig. 2.

Label	Final partition
Peak 1	^{19}F g.s. $(1/2^+) + {}^{39}$K g.s. $(3/2^+)$
	^{19}F$_{0.110}$ $(1/2^-) + {}^{39}$K g.s. $(3/2^+)$
	^{19}F$_{0.197}$ $(5/2^+) + {}^{39}$K g.s. $(3/2^+)$
Peak 2	^{19}F$_{1.345}$ $(5/2^-) + {}^{39}$K g.s. $(3/2^+)$
	^{19}F$_{1.458}$ $(3/2^-) + {}^{39}$K g.s. $(3/2^+)$
	^{19}F$_{1.554}$ $(3/2^+) + {}^{39}$K g.s. $(3/2^+)$
Peak 3	^{19}F g.s. $(1/2^+) + {}^{39}$K$_{2.522}$ $(1/2^+)$
	^{19}F$_{0.110}$ $(1/2^-) + {}^{39}$K$_{2.522}$ $(1/2^+)$
	^{19}F$_{0.197}$ $(5/2^+) + {}^{39}$K$_{2.522}$ $(1/2^+)$
	^{19}F$_{2.779}$ $(9/2^+) + {}^{39}$K g.s. $(3/2^+)$
	^{19}F g.s. $(1/2^+) + {}^{39}$K$_{2.814}$ $(7/2^-)$
	^{19}F$_{0.110}$ $(1/2^-) + {}^{39}$K$_{2.814}$ $(7/2^-)$
	^{19}F$_{0.197}$ $(5/2^+) + {}^{39}$K$_{2.814}$ $(7/2^-)$
	^{19}F g.s. $(1/2^+) + {}^{39}$K$_{3.018}$ $(3/2^-)$
	^{19}F$_{0.110}$ $(1/2^-) + {}^{39}$K$_{3.018}$ $(3/2^-)$
	^{19}F$_{0.197}$ $(5/2^+) + {}^{39}$K$_{3.018}$ $(3/2^-)$
Peak 4	^{19}F g.s. $(1/2^+) + {}^{39}$K$_{3.597}$ $(9/2^-)$
	^{19}F$_{0.110}$ $(1/2^-) + {}^{39}$K$_{3.597}$ $(9/2^-)$
	^{19}F$_{0.197}$ $(5/2^+) + {}^{39}$K$_{3.597}$ $(9/2^-)$
	^{19}F g.s. $(1/2^+) + {}^{39}$K$_{3.883}$ $(5/2^-)$
	^{19}F$_{0.110}$ $(1/2^-) + {}^{39}$K$_{3.883}$ $(5/2^-)$
	^{19}F$_{0.197}$ $(5/2^+) + {}^{39}$K$_{3.883}$ $(5/2^-)$
	^{19}F g.s. $(1/2^+) + {}^{39}$K$_{3.939}$ $(5/2^+)$
	^{19}F$_{0.110}$ $(1/2^-) + {}^{39}$K$_{3.939}$ $(5/2^+)$
	^{19}F$_{0.197}$ $(5/2^+) + {}^{39}$K$_{3.939}$ $(5/2^+)$
	^{19}F g.s. $(1/2^+) + {}^{39}$K$_{3.944}$ $(11/2^-)$
	^{19}F$_{0.110}$ $(1/2^-) + {}^{39}$K$_{3.944}$ $(11/2^-)$
	^{19}F$_{0.197}$ $(5/2^+) + {}^{39}$K$_{3.944}$ $(11/2^-)$
	^{19}F$_{1.345}$ $(5/2^-) + {}^{39}$K$_{2.522}$ $(1/2^+)$
	^{19}F$_{1.345}$ $(5/2^-) + {}^{39}$K$_{2.814}$ $(7/2^-)$
	^{19}F$_{1.345}$ $(5/2^-) + {}^{39}$K$_{3.018}$ $(3/2^-)$
	^{19}F$_{1.458}$ $(3/2^-) + {}^{39}$K$_{2.522}$ $(1/2^+)$
	^{19}F$_{1.458}$ $(3/2^-) + {}^{39}$K$_{2.814}$ $(7/2^-)$
	^{19}F$_{1.458}$ $(3/2^-) + {}^{39}$K$_{3.018}$ $(3/2^-)$
	^{19}F$_{1.554}$ $(3/2^+) + {}^{39}$K$_{2.522}$ $(1/2^+)$
	^{19}F$_{1.554}$ $(3/2^+) + {}^{39}$K$_{2.814}$ $(7/2^-)$
	^{19}F$_{1.554}$ $(3/2^+) + {}^{39}$K$_{3.018}$ $(3/2^-)$
	^{19}F$_{0.110}$ $(1/2^-) + {}^{39}$K$_{4.082}$ $(3/2^-)$
	^{19}F$_{0.197}$ $(5/2^+) + {}^{39}$K$_{4.082}$ $(3/2^-)$
	^{19}F g.s. $(1/2^+) + {}^{39}$K$_{4.096}$ $(1/2^+)$
	^{19}F$_{0.110}$ $(1/2^-) + {}^{39}$K$_{4.096}$ $(1/2^+)$
	^{19}F$_{0.197}$ $(5/2^+) + {}^{39}$K$_{4.096}$ $(1/2^+)$
	^{19}F g.s. $(1/2^+) + {}^{39}$K$_{4.127}$ $(7/2^-)$
	^{19}F$_{0.110}$ $(1/2^-) + {}^{39}$K$_{4.127}$ $(7/2^-)$
	^{19}F$_{0.197}$ $(5/2^+) + {}^{39}$K$_{4.127}$ $(7/2^-)$

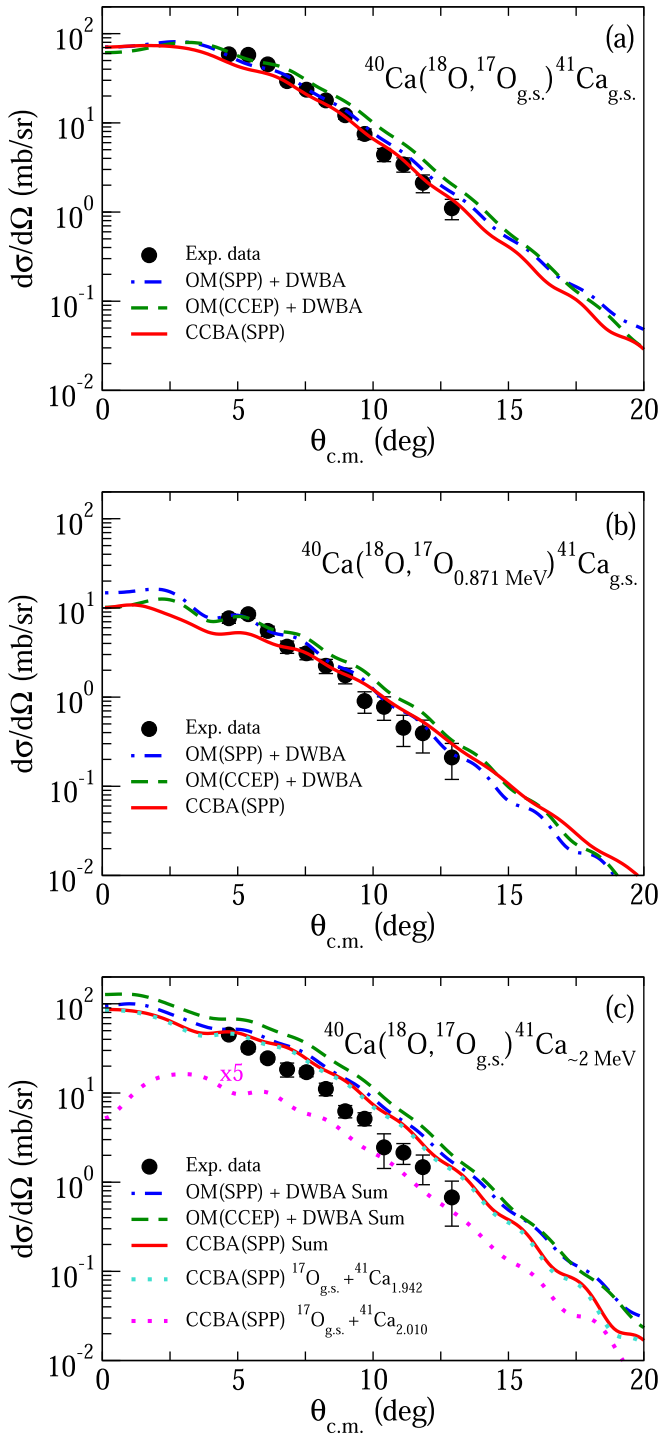

FIG. 3. Comparison between theoretical and experimental one-neutron transfer angular distributions. The different panels refer to the different peaks shown in the excitation energy spectrum of Fig. 1. (a, b) The OM(SPP)+DWBA, OM(CCEP)+DWBA and CCBA(SPP) single-transition calculations are indicated by the dash-dotted blue, dashed green, and solid red lines, respectively. (c) The same symbol code is adopted for the total summed curves whereas the different single transitions, calculated in the CCBA(SPP) scheme, are reported as dotted lines.

interaction potential, and $\langle\psi_b|\psi_a\rangle$ and $\langle\psi_B|\psi_A\rangle$ are the projectile-ejectile and target-residual overlap functions. The latter, assuming the fractional parentage decomposition $B = A + x$ with x the transferred nucleon, can be written as [52]

$$\langle\psi_B|\psi_A\rangle \propto \sum_{nlj} CA_{nlj}\varphi^{xA}_{nlj}(\vec{r}), \tag{2}$$

where C is an isospin Clebsch-Gordan coefficient, A_{nlj} is the spectroscopic amplitude (SA) and $\varphi^{xA}_{nlj}(\vec{r})$ the internal single-particle wave function of x relative to subsystem A. Equations (1) and (2) illustrate that a restricted number of ingredients affects the one-nucleon transfer calculations, namely, the optical potential which determines the distorted waves $\chi^{(\pm)}_{\alpha,\beta}$, the effective potential $V_{\alpha,\beta}$, and the spectroscopic amplitudes A_{nlj}. All of them have represented, in the past, critical quantities when performing nucleon transfer calculations. Nowadays, however, the theoretical and computational refinements have mitigated many sources of uncertainties, allowing to properly tackle transfer calculations in a quite straightforward way.

In the present work, the São Paulo double-folding potential (SPP) [53,54] was adopted as the optical potential in the initial and final partitions. Its effectiveness is indeed already well established since it was systematically tested against a wide range of experimental data [55–57]. Furthermore, SPP was recently employed to analyze, in optical model (OM), DWBA, and coupled channel (CC) schemes, the elastic and inelastic scattering data collected for the identical colliding system at the same bombarding energy of the experiment here examined [39]. In such work as well as in some previous ones [58,59], it was highlighted that, when considering ^{18}O and ^{17}O nuclei, the matter diffuseness value of the Fermi-Dirac density distributions used to generate the potential via the double-folding method should be set to 0.61 fm, increased by about 10% compared to the systematic value of 0.56 fm. Thus, the same prescription was adopted also in the calculations performed in the present case.

The single-particle wave functions are generated adopting, as core effective interactions for the ^{17}O$+n$ and ^{18}O$+p$ systems, Woods-Saxon potentials having a reduced radius (r_0) of 1.25 fm and a diffuseness (a_0) of 0.70 fm. The latter is slightly larger than the typical one used for similar systems ($a_0 = 0.65$ fm) following the same argument introduced to justify the matter diffuseness increase for the optical potentials of the same oxygen isotopes [60]. For the heavier targetlike systems, ^{39}K$+p$ and ^{40}Ca$+n$, $r_0 = 1.20$ fm and $a_0 = 0.60$ fm were adopted, as typically done when considering similar medium-mass nuclei [40]. The depths of such Woods-Saxon potentials were optimized in order to match the experimental one-neutron and one-proton separation energies. The FRESCO code [61,62] was adopted to perform all the described calculations.

The one-neutron and one-proton spectroscopic amplitudes, reported in Tables III and IV, were calculated, for both the projectile and the target overlaps, from large-scale shell-model calculations. Regarding the projectile-ejectile systems, they are performed by means of the shell-model code KSHELL [63] within a model space spanned by the proton and neutron $1p_{3/2}$, $1p_{1/2}$, $2s_{1/2}$, $1d_{5/2}$, and $1d_{3/2}$ orbitals above an ^{4}He core. As an effective Hamiltonian, we have adopted the

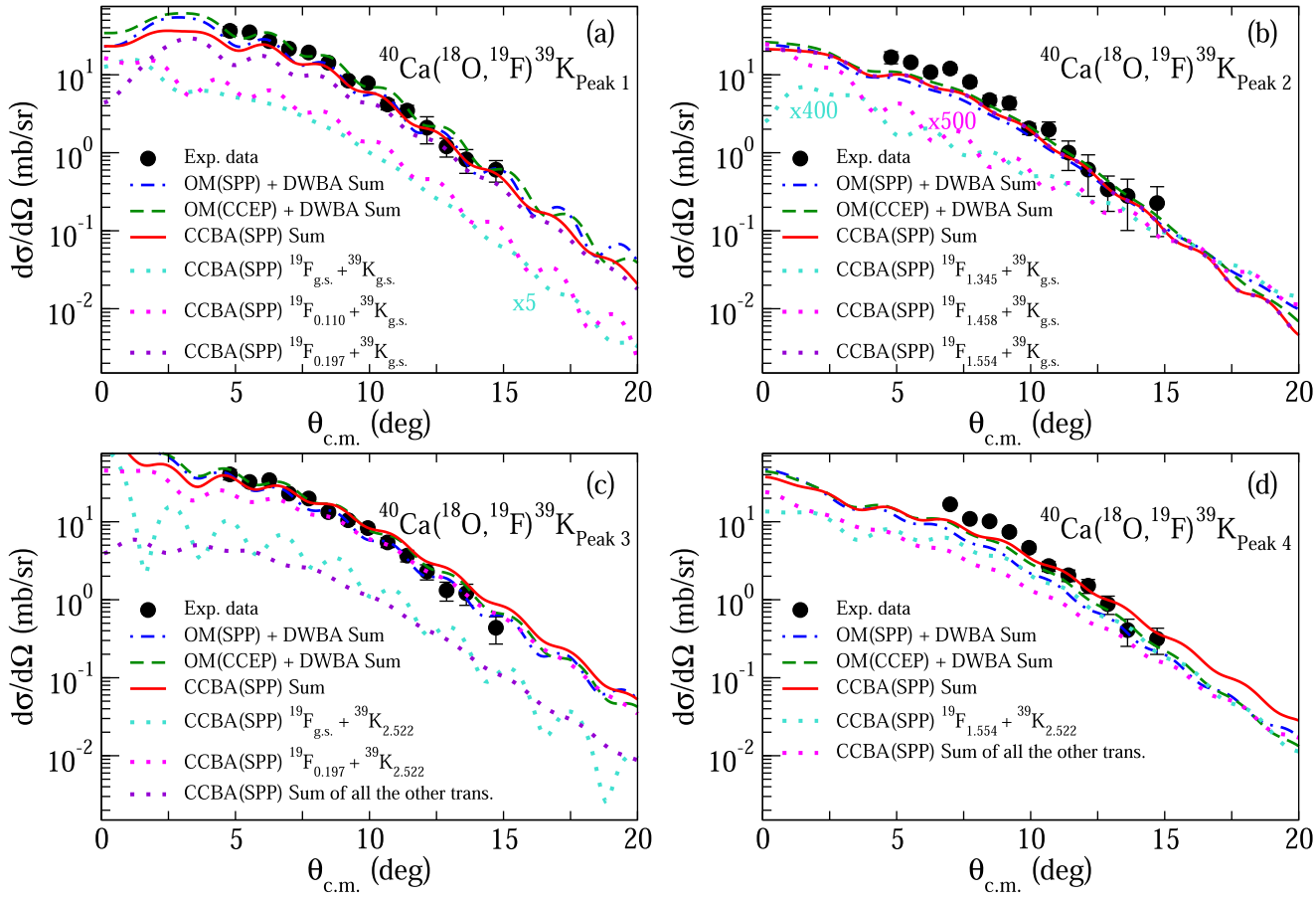

FIG. 4. Comparison between theoretical and experimental one-proton transfer angular distributions. The different panels refer to the different peaks shown in the excitation energy spectrum of Fig. 2. The sum of the OM(SPP)+DWBA, OM(CCEP)+DWBA, and CCBA(SPP) calculations are indicated by the dash-dotted blue, dashed green, and solid red lines, respectively. Single transitions as well as partial sums, calculated in the CCBA(SPP) scheme, are reported as dotted lines.

p-sd-mod interaction [64] which is a modified version of the PSDWBT one [65] to account for multiparticle-multihole states around ^{16}O. This interaction was adopted in several of our previous studies, for instance in Refs. [35,37,60,66–68], to calculate one- and two-nucleon spectroscopic amplitudes and was tested by comparing experimental and theoretical excitation energies of the projectiles and ejectiles involved in the studied reactions [60,67,68]. In particular, in Refs. [35,37,67] it was used to describe oxygen and fluorine nuclei. The spectroscopic amplitudes for the target-residual systems, instead, were computed using the NUSHELLX code [69]. The effective interaction adopted to describe the calcium and potassium isotopes considers a model space composed by the $2s_{1/2}$, $1d_{3/2}$, $1f_{7/2}$, and $2p_{3/2}$ valence orbits for both protons and neutrons on the top of a ^{28}Si core and employs a modified version of the Zucker-Buck-McGrory-2 (ZBM2) effective interaction [70] which was developed from the two-body matrix elements of Ref. [71] in order to describe even and odd Ca isotopes. The ZBM2-modified interaction was also recently used in Ref. [40] to analyze the ^{40}Ca(^{18}O, ^{20}Ne)^{38}Ar transfer reaction. In this paper, the theoretical spectra and electric properties for ^{38}Ar, ^{39}K, and ^{40}Ca were also shown, evidencing a reasonably good agreement with the experimental values.

Both the one-neutron and the one-proton transfer reactions were described within the OM+DWBA and the CCBA frameworks, adopting the prior representation with complex remnant terms. As shown by the schemes sketched in Fig. 5, in the OM+DWBA approach, the couplings between the ground and the excited states of the initial partition are neglected as well as the transfer transitions from such excited states to the final channels of the outgoing partitions. Both these routes, however, could be relevant when considering transfer processes between heavy ions, so they should be included in a reliable calculation. The CCBA, in fact, as schematically shown by the dashed red arrows sketched in Fig. 5, explicitly considers the mentioned couplings in the initial partition and the corresponding additional paths for the transfer transitions. In the performed CCBA calculations, the adopted model space included the first 2^+ excited state at 1.982 MeV for the ^{18}O projectile and the first 3^- and 2^+ states at 3.797 and 3.904 MeV for the ^{40}Ca target (see Fig. 5). It is worth mentioning that the just defined initial partition model space coincides with the one adopted in Ref. [39]. Thus, the reduced matrix elements and deformation lengths [$M(E2) = 6.555\ e\ \text{fm}^2$ and $\delta_2 = 0.921$ fm for the (2_1^+) ^{18}O, $M(E3) = 135.640\ e\ \text{fm}^3$ and $\delta_3 = 2.042$ fm for the (3_1^-) ^{40}Ca, and

TABLE III. List of the one-neutron spectroscopic amplitudes (SAs) adopted in the calculations for the projectile and target overlaps, obtained by shell-model calculations with the p-sd-mod and ZBM2-modified interactions, respectively. The final and initial states as well as the principal quantum number (n), the orbital angular momentum (l), and the spin (j) of the neutron orbitals are reported.

Initial state	Final state	nl_j	SA
^{18}Og.s. (0^+)	^{17}Og.s. $(5/2^+)$	$(1d_{5/2})$	1.2708
	^{17}O$_{0.871}$ $(1/2^+)$	$(2s_{1/2})$	−0.4345
^{18}O$_{1.982}$ (2^+)	^{17}Og.s. $(5/2^+)$	$(1d_{3/2})$	0.0799
		$(1d_{5/2})$	1.0734
		$(2s_{1/2})$	0.5093
	^{17}O$_{0.871}$ $(1/2^+)$	$(1d_{3/2})$	−0.1737
		$(1d_{5/2})$	−0.4994
^{40}Cag.s. (0^+)	^{41}Cag.s. $(7/2^-)$	$(1f_{7/2})$	−0.9376
	^{41}Ca$_{1.942}$ $(3/2^-)$	$(2p_{3/2})$	0.9265
	^{41}Ca$_{2.010}$ $(3/2^+)$	$(1d_{3/2})$	0.3183
^{40}Ca$_{3.737}$ (3^-)	^{41}Cag.s. $(7/2^-)$	$(2s_{1/2})$	−0.3926
		$(1d_{3/2})$	0.4626
	^{41}Ca$_{1.942}$ $(3/2^-)$	$(1d_{3/2})$	−0.1377
	^{41}Ca$_{2.010}$ $(3/2^+)$	$(2p_{3/2})$	0.1499
		$(1f_{7/2})$	−0.3135
^{40}Ca$_{3.904}$ (2^+)	^{41}Cag.s. $(7/2^-)$	$(1f_{7/2})$	−0.1350
		$(2p_{3/2})$	0.0452
	^{41}Ca$_{1.942}$ $(3/2^-)$	$(2p_{3/2})$	−0.0088
		$(1f_{7/2})$	−0.1001
	^{41}Ca$_{2.010}$ $(3/2^+)$	$(2s_{1/2})$	0.4326
		$(1d_{3/2})$	0.3001

$M(E2) = 9.618\ e\ \mathrm{fm}^2$ and $\delta_2 = 0.540$ fm for the (2_1^+) ^{40}Ca], which account for the Coulomb deformations and the nuclear excitations, respectively, were deduced adopting the same prescriptions there reported. Reference [39] highlighted also that, for such a colliding system, when assuming in CC calculations a quite restricted model space like the one presently considered for the initial partition, the optimal strength coefficient for the imaginary part of the corresponding optical potential should be set to 0.78. Another way to implicitly embed the effects of the inelastic excitations on the elastic channel is to resort to a CCEP potential [32]. The latter, obtained by

TABLE IV. List of the one-proton spectroscopic amplitudes (SAs) adopted in the calculations for the projectile and target overlaps, obtained by shell-model calculations with the p-sd-mod and ZBM2-modified interactions, respectively. The final and initial states involved as well as the principal quantum number (n), the orbital angular momentum (l), and the spin (j) of the proton orbitals are reported.

Initial state	Final state	nl_j	SA
^{18}Og.s. (0^+)	^{19}Fg.s. $(1/2^+)$	$(2s_{1/2})$	−0.5539
	^{19}F$_{0.110}$ $(1/2^-)$	$(1p_{1/2})$	−0.2444
	^{19}F$_{0.197}$ $(5/2^+)$	$(1d_{5/2})$	0.6644
	^{19}F$_{1.458}$ $(3/2^-)$	$(1p_{3/2})$	−0.0106
	^{19}F$_{1.554}$ $(3/2^+)$	$(1d_{3/2})$	−0.4238
^{18}O$_{1.982}$ (2^+)	^{19}Fg.s. $(1/2^+)$	$(1d_{5/2})$	−0.5864
		$(1d_{3/2})$	0.2806
	^{19}F$_{0.110}$ $(1/2^-)$	$(1p_{3/2})$	0.0301
	^{19}F$_{0.197}$ $(5/2^+)$	$(1d_{5/2})$	0.4265
		$(1d_{3/2})$	−0.1563
		$(2s_{1/2})$	0.3113
	^{19}F$_{1.345}$ $(5/2^-)$	$(1p_{1/2})$	−0.1366
		$(1p_{3/2})$	−0.0186
	^{19}F$_{1.458}$ $(3/2^-)$	$(1p_{3/2})$	0.0022
		$(1p_{1/2})$	−0.1639
	^{19}F$_{1.554}$ $(3/2^+)$	$(1d_{5/2})$	−0.3146
		$(1d_{3/2})$	−0.3185
		$(2s_{1/2})$	−0.3539
^{40}Cag.s. (0^+)	^{19}F$_{2.779}$ $(9/2^+)$	$(1d_{5/2})$	−0.7872
	^{39}Kg.s. $(3/2^+)$	$(1d_{3/2})$	1.787
	^{39}K$_{2.522}$ $(1/2^+)$	$(2s_{1/2})$	−1.277
	^{39}K$_{2.814}$ $(7/2^-)$	$(1g_{7/2})$	−0.718
	^{39}K$_{3.018}$ $(3/2^-)$	$(2p_{3/2})$	0.223
	^{39}K$_{3.939}$ $(3/2^+)$	$(1d_{3/2})$	0.218
	^{39}K$_{4.082}$ $(3/2^+)$	$(2p_{3/2})$	0.172
	^{39}K$_{4.096}$ $(1/2^+)$	$(2s_{1/2})$	−0.362
	^{39}K$_{4.127}$ $(7/2^-)$	$(1f_{7/2})$	0.245
^{40}Ca$_{3.737}$ (3^-)	^{39}Kg.s. $(3/2^+)$	$(2p_{3/2})$	0.137
		$(1f_{7/2})$	0.538
	^{39}K$_{2.522}$ $(1/2^+)$	$(1f_{7/2})$	0.406
	^{39}K$_{2.814}$ $(7/2^-)$	$(2s_{1/2})$	0.253
		$(1d_{3/2})$	0.847
	^{39}K$_{3.018}$ $(3/2^-)$	$(1d_{3/2})$	−0.017
	^{39}K$_{3.597}$ $(9/2^-)$	$(1d_{3/2})$	0.207
	^{39}K$_{3.883}$ $(5/2^-)$	$(2s_{1/2})$	0.316
		$(1d_{3/2})$	0.629
	^{39}K$_{3.939}$ $(3/2^+)$	$(2p_{3/2})$	0.048
		$(1f_{7/2})$	−0.018
	^{39}K$_{4.082}$ $(3/2^+)$	$(1d_{3/2})$	0.593
	^{39}K$_{4.096}$ $(1/2^+)$	$(1f_{7/2})$	0.080
	^{39}K$_{4.127}$ $(7/2^-)$	$(2s_{1/2})$	0.086
		$(1f_{7/2})$	0.595
^{40}Ca$_{3.904}$ (2^+)	^{39}Kg.s. $(3/2^+)$	$(2s_{1/2})$	−0.030
		$(1d_{3/2})$	−0.008
	^{39}K$_{2.522}$ $(1/2^+)$	$(1d_{3/2})$	−0.014
	^{39}K$_{2.814}$ $(7/2^-)$	$(2p_{3/2})$	0.253
		$(1f_{7/2})$	0.847
	^{39}K$_{3.018}$ $(3/2^-)$	$(2p_{3/2})$	−0.147
		$(1f_{7/2})$	−0.356
	^{39}K$_{3.597}$ $(9/2^-)$	$(1f_{7/2})$	0.260
	^{39}K$_{3.883}$ $(5/2^-)$	$(2p_{3/2})$	−0.026
		$(1f_{7/2})$	−0.174
	^{39}K$_{3.939}$ $(3/2^+)$	$(2s_{1/2})$	−0.153
		$(1d_{3/2})$	−0.464
	^{39}K$_{3.944}$ $(11/2^-)$	$(1f_{7/2})$	0.213
	^{39}K$_{4.082}$ $(3/2^+)$	$(2p_{3/2})$	0.047
		$(1f_{7/2})$	0.234
	^{39}K$_{4.096}$ $(1/2^+)$	$(1d_{3/2})$	0.154
	^{39}K$_{4.127}$ $(7/2^-)$	$(2p_{3/2})$	0.026
		$(1f_{7/2})$	0.249

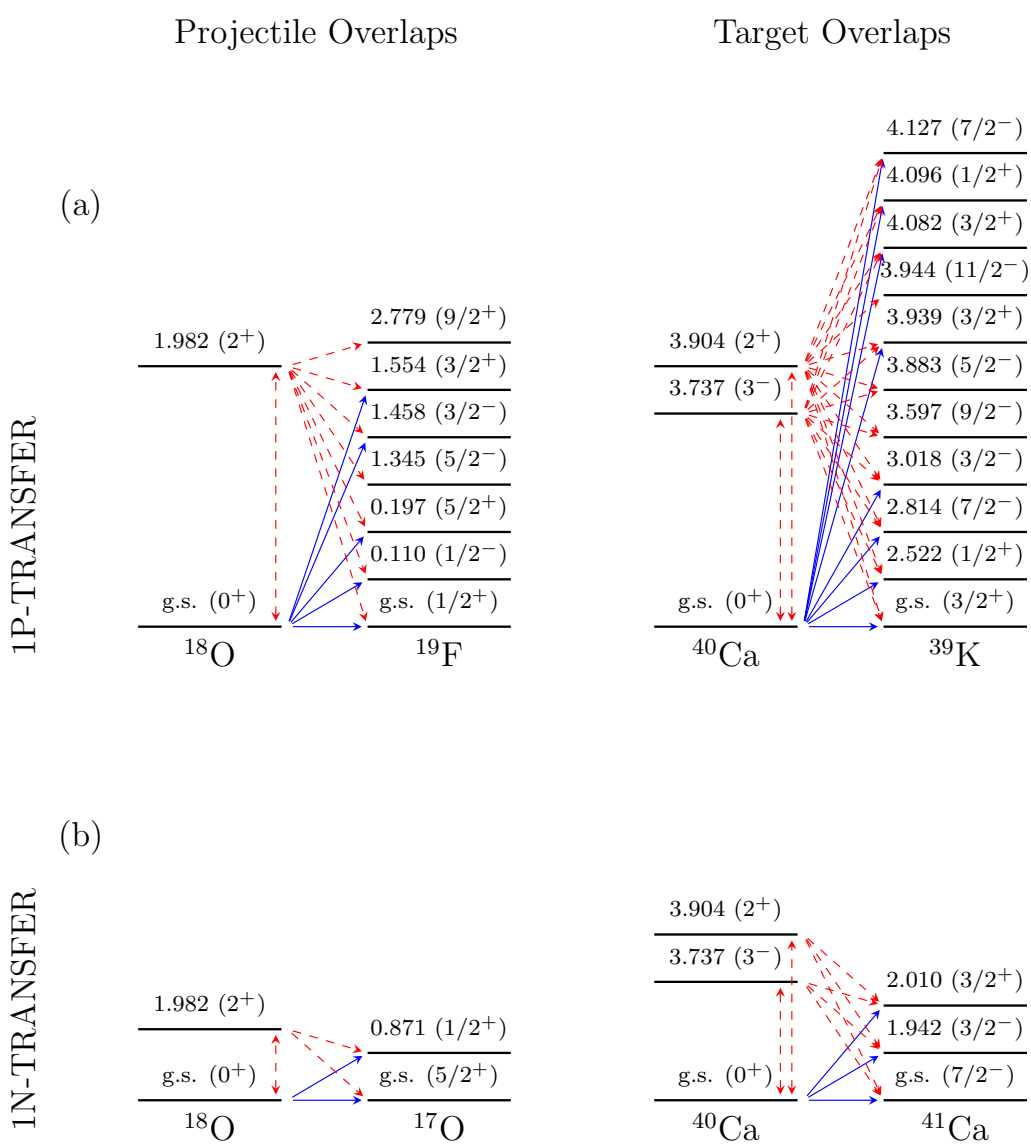

FIG. 5. Coupling schemes for the projectile-ejectile and target-residual systems for the described (a) one-proton and (b) one-neutron transfer reactions. The solid blue arrows refer to the couplings considered only in the OM+DWBA calculations. In the CCBA framework, instead, both the solid blue and the dashed red arrows are included.

adding to the bare optical potential an additive local term known as a trivially equivalent local potential (TELP) [72], includes in an effective way the inelastic couplings among the different considered states, already in the OM scheme [33]. Such an approach was recently tested with success on the $^{18}O + ^{40}Ca$ system elastic transition, which represents its natural test ground, measured at the same kinetic energy of the experiment here presented [39]. In the same paper, moreover, its use was also extended to the direct SCE reactions to effectively introduce, in the corresponding DWBA calculations, the initial partition coupling effects, since any different reaction scheme is not implemented at the moment for the direct heavy-ion SCE. Therefore, it could be interesting also in the one-nucleon transfer reaction case to test and compare the results obtained by such an OM(CCEP)+DWBA approach with the ones given by the traditional OM(SPP)+DWBA and CCBA(SPP) schemes.

IV. ^{40}Ca(^{18}O, ^{17}O)^{41}Ca ONE-NEUTRON TRANSFER RESULTS

The cross section angular distributions for the ^{40}Ca(^{18}O, ^{17}O)^{41}Ca reaction are shown in Fig. 3. In Fig. 3(a) the transition to $^{17}O_{g.s.}(5/2^+) + ^{41}Ca_{g.s.}(7/2^-)$ is considered. An almost structureless shape with an exponential decrease is observed, also typical of the ^{18}O beam impinging at similar bombarding energy on different medium-mass targets [34]. The OM(SPP)+DWBA, OM(CCEP)+DWBA, and CCBA(SPP) calculation results are quite similar, with the CCBA(SPP) distribution presenting a slightly steeper slope than the OM(SPP)+DWBA and OM(CCEP)+DWBA ones, which better reproduces the experimental trend at large angles. Similar considerations can be extended to the cross section angular distributions corresponding to the excitation of the $^{17}O_{0.871}(1/2^+) + ^{41}Ca_{g.s.}(7/2^-)$ channel, shown in

Fig. 3(b). The OM(SPP)+DWBA and OM(CCEP)+DWBA calculations well describe the data in the most forward angular region, slightly overestimating them, instead, at larger angles. The CCBA(SPP) distribution presents a different slope which is less steep than the OM(SPP)+DWBA and OM(CCEP)+DWBA trends. The third angular distribution plotted in Fig. 3(c) refers to the excitation of both $^{17}O_{g.s.}(5/2^+) + {}^{41}Ca_{1.942}(3/2^-)$ and $^{17}O_{g.s.}(5/2^+) + {}^{41}Ca_{2.010}(3/2^+)$ final channels, respectively. The summed curves are practically exhausted by the transition towards the $^{41}Ca(3/2^-)$ state, since the contribution from the $(3/2^+)$ one is about one order of magnitude lower. This result is not entirely surprising since the weakness of the transition to the state at 2.010 MeV was also observed in light-ion-induced transfer reactions at low and intermediate bombarding energies [73,74]. Comparing the results provided by the different reaction schemes, it can be observed that OM(SPP)+DWBA and OM(CCEP)+DWBA are very similar. The coupled channel terms introduced in the CCBA(SPP) calculation, instead, slightly decrease the final distribution, improving the matching with the experimental data.

Generally, it can be noticed that, for the one-neutron transfer results just discussed, the agreement with the experimental data is quite satisfactory, validating the employed nuclear structure and reaction models and confirming that absolute agreements can be reached without the need for any arbitrary scaling. Moreover, the different adopted reaction schemes return similar results, demonstrating a substantial equivalence among the different approaches.

V. ^{40}Ca (^{18}O, ^{19}F) ^{39}K ONE-PROTON TRANSFER RESULTS

The cross section angular distributions for the $^{40}Ca(^{18}O, {}^{19}F)\,{}^{39}K$ reactions are presented in Fig. 4. Regarding peak 1 and peak 2 shown in Fig. 2 and located in the g.s. region and at about 1.4 MeV, three transitions are expected to contribute to each one (see Table II). They correspond to as many ^{19}F states, since for the ^{39}K residual nucleus no nuclear state different from its g.s. lies in such energy regions.

For peak 1, as shown in Fig. 4(a), the transition toward the $^{19}F(5/2^+)$ state at 0.197 MeV is expected to dominate over the other two, the $(1/2^+)$ g.s. and the $(1/2^-)$ state at 0.110 MeV, shifting the centroid of peak 1 at about 200 keV. The obtained result reflects the corresponding theoretical SA values (see Table IV). In particular, the ratio between the $(1/2^-)$ and the $(5/2^+)$ ones is close to the one experimentally extracted from a previous spectroscopic study of ^{19}F [75]. The differences among the calculations performed in OM(SPP)+DWBA, OM(CCEP)+DWBA, and CCBA(SPP) are very small. In the angular region explored by the present data, the OM(CCEP)+DWBA distribution is slightly larger than the OM(SPP)+DWBA one, showing also a similar oscillation pattern. The CCBA(SPP) distribution is found to be lower than the other two calculations at small scattering angles, also presenting the smoothest trend. In any case, within all the different theoretical schemes, the agreement between calculations and experimental data is highly satisfactory.

The angular distribution for peak 2, shown in Fig. 4(b), is practically exhausted by just one of the three possible transitions, the one toward the $(3/2^+)$ state at 1.554 MeV, which has been strongly excited also in similar heavy-ion collisions [34,37]. Indeed, the angular distributions due to the $(5/2^-)$ state at 1.345 MeV and the $(3/2^-)$ at 1.458 MeV are more than three orders of magnitude smaller. This is not surprising examining the corresponding SA, also for the two-step transitions via the $^{18}O_{1.982}$ state which are expected to be quite suppressed. In the present calculations, in particular, the contribution from the $(3/2^-)$ state at 1.458 MeV was included only in the CCBA(SPP) calculation. In fact, the corresponding OM(SPP)+DWBA spectroscopic amplitude cannot be provided within the adopted shell-model space, considering that such a state cannot be populated from the $^{18}O_{g.s.}$ (0^+). Examining the results performed with the different reaction models, it can be noticed that also in this energy region the OM(CCEP)+DWBA distribution is slightly larger than the OM(SPP)+DWBA one in the range explored by the presented experimental data. The CCBA(SPP) calculation lies between the two DWBA distributions up to $\approx 15^\circ$, then showing more pronounced oscillations.

In peaks 3 and 4 the number of the involved channels of the final partition is significantly larger than in the previous cases since both the ejectile (^{19}F) and the residual nucleus (^{39}K) may populate many possible excited states in the corresponding energy ranges (see Table II). Namely, peak 3 can receive contributions from ten final partition channels. Nevertheless, as it is shown in Fig. 4(c) and was already observed in the previous energy ranges, few transitions dominate over all the others. In particular, the $^{19}F_{0.197}(5/2^+) + {}^{39}K_{2.522}(1/2^+)$ final transition gives the largest contribution while a limited enhancement in the oscillation pattern is provided by the transition towards the $^{19}F_{g.s.}(1/2^+) + {}^{39}K_{2.522}(1/2^+)$ final channel which, according to previous spectroscopic study, is expected to contain most of the $2s_{1/2}$ strength [76]. The sum of all the other transitions gives a suppressed and almost constant contribution. Comparing the results obtained applying the different theoretical schemes, the OM(SPP)+DWBA is slightly smaller than the OM(CCEP)+DWBA distribution as already seen in previous energy regions, providing an excellent agreement with the data in both cases. The CCBA(SPP) angular distribution is instead higher than the others especially at large scattering angles, slightly overestimating the experimental result.

Finally, peak 4 receives contributions from many considered final partition channels, which are listed in Table II. However, similarly to what has already seen in case of peak 3, only a few of them dominate over all the others. In particular, in the experimentally explored angular region, the $^{19}F_{1.554}(1/2^+) + {}^{39}K_{2.522}(1/2^+)$ channel accounts for about 60% of the total cross section while the sum of all the other transitions amounts to the remaining 40%. Comparing the different distributions, in this case a significant discrepancy is observed between the experimental data and the OM(SPP)+DWBA curve, which is partially recovered by the OM(CCEP)+DWBA one and to a larger extent by the CCBA(SPP) distribution.

Generally, it can be noticed that, for the one-proton transfer results, the agreement with the experimental data can be judged satisfactory, considering that also in this case no

arbitrary factors have been introduced in the calculations. The present analysis confirms also the dominant role, in the explored portion of the energy spectra, of the transitions to specific low-lying states of ^{19}F and ^{39}K. Namely, the $(5/2^+)$ state at 0.197 MeV and the $(3/2^+)$ state at 1.554 MeV are strongly populated for the ^{19}F ejectiles, while the $(3/2^+)$ g.s. and the $(1/2^+)$ state at 2.522 MeV are involved for the ^{39}K residual nuclei. This result is a consequence of the dominant single-particle configuration of the mentioned ^{19}F states and single-hole configuration for the ^{39}K ones, reflected by the large SA for such configurations. Despite that this result could appear not surprising, it is interesting anyway as it indicates a clear selectivity of the studied (^{18}O, ^{19}F) proton pickup reaction, a feature which is not much known for heavy-ion-induced processes above the Coulomb barrier. Moreover, from the present analysis, it turned out that also the simplest OM(SPP)+DWBA scheme can acceptably reproduce the experimental distributions, at least in the first three excitation energy regions (peaks 1, 2, and 3) which extend up to about 3 MeV. The theoretical results obtained within the more complete and sophisticated OM(CCEP)+DWBA and CCBA(SPP) frameworks, indeed, are very similar to each other. In the case of peak 4, instead, a discrepancy between the experimental data and the OM(SPP)+DWBA curve is observed. Such a result is not surprising, since this distribution corresponds to the experimental peak located at the highest excitation energy ($\approx$4 MeV) among the analyzed structures. Thus, it includes those transitions which are expected to receive the largest contributions from the transfer processes originating from the initial partition excited states, which are not included in the OM(SPP)+DWBA scheme. As a partial confirmation of this argument, the observed discrepancy in the angular distribution of peak 4 is only partially recovered when just the effects of the initial partition excited states are effectively incorporated as done in the OM(CCEP)+DWBA calculation. The agreement is improved performing the CCBA(SPP), where the transfer paths from also the inelastic states are included.

VI. CONCLUSIONS

The ^{40}Ca(^{18}O, ^{17}O)^{41}Ca one-neutron stripping and the ^{40}Ca(^{18}O, ^{19}F)^{39}K one-proton pickup reactions induced by an ^{18}O beam at 15.3A MeV on a ^{40}Ca target were investigated, both experimentally and theoretically. They complete the analysis of the interesting reaction channels explored so far for the ^{40}Ca target within the NUMEN project. Several structures were identified in the corresponding excitation energy spectra and their angular cross sections distributions were extracted. The theoretical calculations were performed adopting different reaction frameworks: OM(SPP)+DWBA, OM(CCEP)+DWBA, and CCBA(SPP). To reduce the model dependency of such theoretical results, the nuclear parameters entering in the calculations were constrained on the basis of complementary analyses involving other reaction channels investigated in the same experimental conditions. Indeed, all the main parameters used in the present calculations are constrained by other data analyses, such as for the elastic and inelastic scattering [39] and two-proton transfer reaction [40], thus refining the reaction and nuclear structure model responses provided within the available systematics. The latter point confirms that, in the present multichannel framework, the adopted physical quantities and models needed to perform a modern nucleon transfer calculation are under control without resorting to any arbitrary scaling.

Comparing the results obtained with the different reaction schemes, it emerges that, in the present experimental conditions, the coupling effects to the first low-lying excited states and the two-step contributions are quite suppressed. Such a result demonstrates that, for the reaction system under investigation, also the simplest DWBA scheme represents a suitable framework to analyze such heavy-ion nucleon transfer reactions. This may be connected to the doubly magic nature of the ^{40}Ca nucleus, so this behavior is not necessarily universal. The results obtained within the OM(CCEP)+DWBA framework are, for both the reactions under investigation, very similar to the ones reached with the OM(SPP)+DWBA approach. Therefore, no apparent significant difference exists between the two approximations for the considered transfer reactions.

Finally, the present results here obtained set the stage, under the same experimental and theoretical conditions, to an accurate and reliable analysis of the sequential-nucleon transfer processes in competition with the charge exchange reactions.

ACKNOWLEDGMENTS

The authors wish to thank the operators of INFN-LNS Accelerator Division for the production and delivery of the ^{18}O beam and their support throughout the experiment. The research leading to these results was partially funded by the European Research Council (ERC) under the European Union's Horizon 2020 Research and Innovation Programme (Grant Agreement No. 714625). We also acknowledge the CINECA award under the ISCRA initiative through the INFN-CINECA agreement for the availability of high performance computing resources and support. G.D.G. acknowledges the support by the funding program VALERE of Università degli Studi della Campania "Luigi Vanvitelli". Brazilian authors thank the partial financial support from Instituto Nacional de Ciência e Tecnologia - Física Nuclear e Aplicações (Proc. No. 464898/2014-5), Conselho Nacional de Desenvolvimento Científico e Tecnológico, Fundação de Amparo à Pesquisa no Estado de Rio de Janeiro and Fundação de Amparo à Pesquisa no Estado de São Paulo (Proc. No. 2019/07767-1). J.A.L. acknowledges support by the Spanish Ministerio de Ciencia, Innovación y Universidades and FEDER funds under Project No. FIS2017-88410-P.

[1] M. H. Macfarlane and J. B. French, Rev. Mod. Phys. **32**, 567 (1960).
[2] S. T. Butler, Proc. R. Soc. London **208**, 559 (1951).
[3] S. Kahana and A. Baltz, Adv. Nucl. Phys. **9**, 1 (1977).
[4] W. von Oertzen and A. Vitturi, Rep. Prog. Phys. **64**, 1247 (2001).

[5] G. Potel *et al.*, Rep. Prog. Phys. **76**, 106301 (2013).
[6] F. Cappuzzello *et al.*, Nat. Commun. **6**, 6743 (2015).
[7] M. C. Mermaz, in *Proceedings of 17th International Winter Meeting on Nuclear Physics (Bormio 1979): Bormio, Italy*, edited by I. Iori (Milan University, Bormio (SO), Italy, 1979), Vol. 4549.
[8] P. Kunz, J. Vaagen, J. Bang, and B. Nilsson, Phys. Lett. B **112**, 5 (1982).
[9] H. Oberhummer, W. Pfeifer, F. Brunner, and H. Müller, Nucl. Phys. A **401**, 415 (1983).
[10] P. Kunz, T. Kammuri, and H. Shimaoka, Nucl. Phys. A **376**, 401 (1982).
[11] F. Brunner, H. Müller, C. Dorninger, and H. Oberhummer, Nucl. Phys. A **398**, 84 (1983).
[12] X. D. Liu, M. A. Famiano, W. G. Lynch, M. B. Tsang, and J. A. Tostevin, Phys. Rev. C **69**, 064313 (2004).
[13] J. Lee, M. B. Tsang, and W. G. Lynch, Phys. Rev. C **75**, 064320 (2007).
[14] A. Parmar *et al.*, Nucl. Phys. A **940**, 167 (2015).
[15] M. B. Tsang, J. Lee, and W. G. Lynch, Phys. Rev. Lett. **95**, 222501 (2005).
[16] H. Lenske, H. H. Wolter, and H. G. Bohlen, Phys. Rev. Lett. **62**, 1457 (1989).
[17] C. H. Dasso and A. Vitturi, Phys. Rev. C **34**, 743 (1986).
[18] F. Cappuzzello *et al.*, Nucl. Phys. A **739**, 30 (2004).
[19] J. Bang, F. Gareev, S. Goncharov, and G. Kasaca, Nucl. Phys. A **429**, 330 (1984).
[20] J. Cook, K. W. Kemper, P. V. Drumm, L. K. Fifield, M. A. C. Hotchkis, T. R. Ophel, and C. L. Woods, Phys. Rev. C **30**, 1538 (1984).
[21] N. Clarke and J. Cook, Nucl. Phys. A **458**, 137 (1986).
[22] S. Nakayama *et al.*, Phys. Lett. B **246**, 342 (1990).
[23] L. Fifield *et al.*, Nucl. Phys. A **552**, 125 (1993).
[24] F. Cappuzzello *et al.*, Eur. Phys. J. A **54**, 72 (2018).
[25] C. Agodi *et al.*, Nucl. Part. Phys. Proc. **265-266**, 28 (2015).
[26] C. Agodi *et al.*, Universe **7**, 72 (2021).
[27] F. Cappuzzello *et al.*, Front. Astron. Space Sci. **8**, 52 (2021).
[28] J. I. Bellone *et al.*, Phys. Lett. B **807**, 135528 (2020).
[29] H. Lenske, J. Bellone, M. Colonna, and D. Gambacurta, Universe **7**, 98 (2021).
[30] H. Lenske, F. Cappuzzello, M. Cavallaro, and M. Colonna, Prog. Part. Nucl. Phys. **109**, 103716 (2019).
[31] R. J. Ascuitto and N. K. Glendenning, Phys. Rev. **181**, 1396 (1969).
[32] I. Thompson, M. Nagarajan, J. Lilley, and B. Fulton, Phys. Lett. B **157**, 250 (1985).
[33] J. Rangel, J. Lubian, L. F. Canto, and P. R. S. Gomes, Phys. Rev. C **93**, 054610 (2016).
[34] M. A. G. Fernandes, B. L. Burks, D. J. Horen, G. R. Satchler, R. L. Auble, F. E. Bertrand, J. L. Blankenship, J. L. C. Ford, Jr., E. E. Gross, D. C. Hensley, R. O. Sayer, D. Shapira, and T. P. Sjoreen, Phys. Rev. C **33**, 1971 (1986).
[35] E. Crema, V. A. B. Zagatto, J. M. B. Shorto, B. Paes, J. Lubian, R. F. Simões, D. S. Monteiro, J. F. P. Huiza, N. Added, M. C. Morais, and P. R. S. Gomes, Phys. Rev. C **98**, 044614 (2018).
[36] R. Linares, M. J. Ermamatov, J. Lubian, F. Cappuzzello, D. Carbone, E. N. Cardozo, M. Cavallaro, J. L. Ferreira, A. Foti, A. Gargano, B. Paes, G. Santagati, and V. A. B. Zagatto, Phys. Rev. C **98**, 054615 (2018).
[37] O. Sgouros, M. Cavallaro, F. Cappuzzello, D. Carbone, C. Agodi, A. Gargano, G. De Gregorio, C. Altana, G. A. Brischetto, S. Burrello, S. Calabrese, D. Calvo, V. Capirossi, E. R. Chávez Lomeli, I. Ciraldo, M. Cutuli, F. Delaunay, H. Djapo, C. Eke, P. Finocchiaro, M. Fisichella, A. Foti, A. Hacisalihoglu, F. Iazzi, L. La Fauci, R. Linares, J. Lubian, N. H. Medina, M. Moralles, J. R. B. Oliveira, A. Pakou, L. Pandola, F. Pinna, G. Russo, M. A. Guazzelli, V. Soukeras, G. Souliotis, A. Spatafora, D. Torresi, A. Yildirim, and V. A. B. Zagatto, Phys. Rev. C **104**, 034617 (2021).
[38] R. H. Siemssen, C. L. Fink, L. R. Greenwood, and H. J. Körner, Phys. Rev. Lett. **28**, 626 (1972).
[39] M. Cavallaro *et al.*, Front. Astron. Space Sci. **8**, 61 (2021).
[40] J. L. Ferreira, D. Carbone, M. Cavallaro, N. N. Deshmukh, C. Agodi, G. A. Brischetto, S. Calabrese, F. Cappuzzello, E. N. Cardozo, I. Ciraldo, M. Cutuli, M. Fisichella, A. Foti, L. La Fauci, O. Sgouros, V. Soukeras, A. Spatafora, D. Torresi, and J. Lubian (NUMEN Collaboration), Phys. Rev. C **103**, 054604 (2021).
[41] F. Cappuzzello *et al.*, Eur. Phys. J. A **51**, 145 (2015).
[42] E. Santopinto, H. García-Tecocoatzi, R. I. Magaña Vsevolodovna, and J. Ferretti (NUMEN Collaboration), Phys. Rev. C **98**, 061601(R) (2018).
[43] F. Cappuzzello, C. Agodi, D. Carbone, and M. Cavallaro, Eur. Phys. J. A **52**, 167 (2016).
[44] D. Torresi *et al.*, Nucl. Instrum. Methods Phys. Res., Sect. A **989**, 164918 (2021).
[45] M. Cavallaro *et al.*, Eur. Phys. J. A **48**, 59 (2012).
[46] F. Cappuzzello *et al.*, Nucl. Instrum. Methods Phys. Res., Sect. A **621**, 419 (2010).
[47] F. Cappuzzello, D. Carbone, and M. Cavallaro, Nucl. Instrum. Methods Phys. Res., Sect. A **638**, 74 (2011).
[48] M. Cavallaro *et al.*, Nucl. Instrum. Methods Phys. Res., Sect. A **637**, 77 (2011).
[49] F. Cappuzzello *et al.*, Nucl. Instrum. Methods Phys. Res., Sect. A **763**, 314 (2014).
[50] D. Carbone, Eur. Phys. J. Plus **130**, 143 (2015).
[51] G. R. Satchler, *Direct Nuclear Reactions* (Clarendon Press, Oxford, 1983).
[52] E. Kwasniewicz, H. Herndl, and H. Oberhummer, J. Phys. G: Nucl. Part. Phys. **20**, 1919 (1994).
[53] L. C. Chamon, B. V. Carlson, L. R. Gasques, D. Pereira, C. De Conti, M. A. G. Alvarez, M. S. Hussein, M. A. Cândido Ribeiro, E. S. Rossi, Jr., and C. P. Silva, Phys. Rev. C **66**, 014610 (2002).
[54] L. Chamon, in *Proceedings of the Ninth International Conference on Nucleus-Nucleus Collisions*, special issue of Nucl. Phys. A **787**, 198 (2007).
[55] M. Alvarez *et al.*, Nucl. Phys. A **723**, 93 (2003).
[56] D. Pereira *et al.*, Phys. Lett. B **670**, 330 (2009).
[57] D. Carbone *et al.*, Universe **7**, 58 (2021).
[58] J. F. P. Huiza, E. Crema, A. Barioni, D. S. Monteiro, J. M. B. Shorto, R. F. Simões, and P. R. S. Gomes, Phys. Rev. C **82**, 054603 (2010).
[59] E. Crema, D. R. Otomar, R. F. Simões, A. Barioni, D. S. Monteiro, L. K. Ono, J. M. B. Shorto, J. Lubian, and P. R. S. Gomes, Phys. Rev. C **84**, 024601 (2011).
[60] E. N. Cardozo, J. Lubian, R. Linares, F. Cappuzzello, D. Carbone, M. Cavallaro, J. L. Ferreira, A. Gargano, B. Paes, and G. Santagati, Phys. Rev. C **97**, 064611 (2018).
[61] I. J. Thompson, Comput. Phys. Rep. **7**, 167 (1988).

[62] I. Thompson, http://www.fresco.org.uk/.
[63] N. Shimizu, T. Mizusaki, Y. Utsuno, and Y. Tsunoda, Comput. Phys. Commun. **244**, 372 (2019).
[64] Y. Utsuno and S. Chiba, Phys. Rev. C **83**, 021301(R) (2011).
[65] E. K. Warburton and B. A. Brown, Phys. Rev. C **46**, 923 (1992).
[66] R. Linares, C. C. Seabra, V. A. B. Zagatto, V. Scarduelli, L. Gasques, L. C. Chamon, B. R. Gonçalves, D. R. M. Junior, and A. Lépine-Szily, Phys. Rev. C **101**, 014611 (2020).
[67] D. Carbone, J. L. Ferreira, S. Calabrese, F. Cappuzzello, M. Cavallaro, A. Hacisalihoglu, H. Lenske, J. Lubian, R. I. Magnaña Vsevolodovna, E. Santopinto, C. Agodi, L. Acosta, D. Bonanno, T. Borello-Lewin, I. Boztosun, G. A. Brischetto, S. Burrello, D. Calvo, E. R. Chávez Lomeli, I. Ciraldo, M. Colonna, F. Delaunay, N. Deshmukh, P. Finocchiaro, M. Fisichella, A. Foti, G. Gallo, F. Iazzi, L. La Fauci, G. Lanzalone, R. Linares, N. H. Medina, M. Moralles, J. R. B. Oliveira, A. Pakou, L. Pandola, H. Petrascu, F. Pinna, S. Reito, G. Russo, O. Sgouros, S. O. Solakci, V. Soukeras, G. Souliotis, A. Spatafora, D. Torresi, S. Tudisco, A. Yildirin, and V. A. B. Zagatto, Phys. Rev. C **102**, 044606 (2020).
[68] D. Carbone, J. L. Ferreira, F. Cappuzzello, J. Lubian, C. Agodi, M. Cavallaro, A. Foti, A. Gargano, S. M. Lenzi, R. Linares, and G. Santagati, Phys. Rev. C **95**, 034603 (2017).
[69] W. Rae, http://www.garsington.eclipse.co.uk (2008).
[70] E. Caurier *et al.*, Phys. Lett. B **522**, 240 (2001).
[71] J. Retamosa, E. Caurier, F. Nowacki, and A. Poves, Phys. Rev. C **55**, 1266 (1997).
[72] I. Thompson, M. Nagarajan, J. Lilley, and M. Smithson, Nucl. Phys. A **505**, 84 (1989).
[73] L. L. Lee *et al.*, Phys. Rev. **136**, B971 (1964).
[74] H. Niewodniczanski, J. Nurzynski, A. Strzalkowski, and G. R. Satchler, Phys. Rev. **146**, 799 (1966).
[75] L. Green, C. Lennon, and I. Naqib, Nucl. Phys. A **142**, 137 (1970).
[76] D. W. Devins, D. L. Friesel, W. P. Jones, A. C. Attard, S. F. Collins, G. G. Shute, B. M. Spicer, V. C. Officer, I. D. Svalbe, R. S. Henderson, and W. E. Dollhopf, Phys. Rev. C **24**, 59 (1981).